5 Density and refractive index

In this chapter we describe precision measurements of the refractive index and the density of SF_6 in a region around the critical density. The refractive index is determined with the help of the IFU as described in section 3.3 and the density is determined in the traditional way. Previously, either the density or the refractive index was determined experimentally and the Lorentz–Lorenz relation [42] was used to find the one quantity out of the other. However, the Lorentz–Lorenz relation is only approximate and it was far from evident that this approximation is sufficiently accurate for our purpose [75]. Our results show that the Lorentz–Lorenz relation is not suited to describe this relation around the critical density with the accuracy we desire.

5.1 Linearity of n(ρ) dependence

In order to determine density changes in a fluid by measuring the change in interference order in an interferogram (eq. (4.1)), an accurate relation between n and ρ for the density range of interest is required. It is generally assumed that this relation is most accurately given [42] by the Lorentz–Lorenz expression:

$$\frac{n^2-1}{n^2+2} = Q\rho\,, \tag{5.1}$$

where Q is the Lorentz–Lorenz constant dependent only on the fluid system. By expanding eq. (5.1) around the critical density, one obtains

$$n = n_c + \frac{\rho-\rho_c}{\rho_c}\frac{\left(n_c^2-1\right)\left(n_c^2+2\right)}{6n_c} + \left(\frac{\rho-\rho_c}{\rho_c}\right)^2\frac{\left(n_c^2-1\right)^2\left(n_c^2+2\right)\left(3n_c^2-2\right)}{72n_c^3} + \ldots\,, \tag{5.2}$$

where n_c is the critical refractive index. Using literature values for n_c and ρ_c one finds that for the density range $0.5\rho_c < \rho < 1.5\rho_c$ the Lorentz–Lorenz expression is approximated, with a precision better than 1%, by the linear relation

$$n - n_c = C\phi, \tag{5.3}$$

where

$$C \equiv \frac{(n_c^2 - 1)(n_c^2 + 2)}{6n_c}. \tag{5.4}$$

For the density range $0.95\rho_c < \rho < 1.05\rho_c$ the precision is even better than 1‰. Literature values of the critical point are given in table 5.1.

Equation (5.3) suggests that the relation between the density and the refractive index around the liquid-vapour critical point is fixed completely by the values for n_c and ρ_c. If knowledge of the Lorentz–Lorenz constant is presumed, determination of either n_c or ρ_c then suffices to fully establish the $n(\rho)$-relation. However, although obviously it is possible to linearize around ρ_c, this chapter will show that on the basis of the Lorentz–Lorenz relation a wrong slope is found for the $n(\rho)$-relation. This in contrast to what usually is assumed in the literature. It was found that our data for n versus ρ cannot be described within experimental accuracy by the Lorentz–Lorenz relation.

When eq. (5.3) may be applied, eq. (4.1) shows that a simple linear relation exists between interference order and density in the critical region:

$$\Delta k = F\Delta\rho, \tag{5.5}$$

where $F \equiv \frac{LC}{\Lambda\rho_c}$.

Table 5.1 Critical values for SF_6.

author(s)		T_c (K)	ρ_c (kg/m^3)	n_c (-)	Q (m^3/kg)	sample purity (mol%)
		318.78	725	-		99.9
Wentorf [76]	(1955)	318.82	740	-		99.9
Makarevich et al. [77]	(1968)	318.71	738.7	-		99.995
Rathjen et al. [78]	(1973)	318.63	740	-		99.95
Kijima [79]	(1973)	318.78	725	-		99.994
Watanabe et al. [80]	(1977)	318.70	740	-		99.997
Huijser et al. [69]	(1983)	318.697	730	1.093	$8.35\cdot10^{-5}$	-
Jany and Straub [36]	(1987)	318.68	741	1.0891	$7.88\cdot10^{-5}$	-
Klein and Feuerbacher [19]	(1987)	318.70	730	-		-
Biswas and Ten Seldam [33]	(1989)	318.71	745	-		99.993
Wyczalkowska et al. [81]	(1997)	318.727	742	-		-
this work	(1998)	-	740.5	1.08712	$7.717\cdot10^{-5}$	99.998

5.2 Experimental procedure

The measurements for this experiment were performed in the CPF thermostat with the DER-SCU (see section 3.3.3), using the laboratory equipment (section 3.2). As with all the experiments described in this thesis, SF_6 was obtained from the firm Messer Griesheim in Duisburg, Germany, with a guaranteed purity of 99.998 Vol.%. The foreign residue consists mainly of oxygen (<5 vpm), nitrogen (<5 vpm), water (<2 vpm), fluorhydrogen (<0.1 vpm) and tetrafluormethane (<5 vpm).

The basic steps in an experimental run are evacuating the SCU, then filling it to close to critical density during which the refractive index (n) is monitored, and finally measuring the actual density ρ and the position z_m of the meniscus with respect to the volumetric middle of the container, which is a measure of the distance to ρ_c ($z_m \sim (\rho - \rho_c)$, see section 2.4.3). The actual experimental scenario incorporated 17 runs of different densities around the critical density, but, as explained hereafter not all steps were executed on each run.

The position of the meniscus is determined at two temperatures slightly below T_c, respectively T_c-110 mK and T_c-30 mK. Since, for a density slightly off-critical, the meniscus moves away from the middle when the temperature is raised, in principal the distance to CP may be determined more accurately closer to T_c †. However, closer to CP the fluid is more susceptible to small disturbances, such as heat absorption from the light beam. Moreover, there is the problem of increase of the time needed for system equilibration, due to the well-known critical slowing down. Therefore, the increase in resolution of the meniscus position will be counteracted by a decrease in accuracy because of these effects. These may, of course, also affect the sample at the temperatures chosen; since, however, the impact cannot be determined a priori, we have let the analysis of the data decide on this issue.

The density of each sample is calculated out of the sample mass and the total volume of the chamber. The latter is known with great accuracy (0.25‰, see section 3.3.3). The mass of the sample was found by determining the difference in weight between the evacuated SCU and the SCU with its sample. The weighing was performed utilizing a Mettler balance type B5C1000, in principle capable of weighing with an accuracy of 0.1 mg. Since the weighing is influenced by a change in either the temperature, the density or the humidity of the air, or in atmospheric pressure, great care has to be taken to keep the environment conditions for the SCU as constant as possible during and in between the weighing. Moreover, the sample mass is only about 1.25% of that of the SCU. As a consequence, in the determination of sample mass this high accuracy is never obtained. A more realistic figure is about 5 mg, equivalent to an uncertainty of 0.5‰.

The refractive index is determined by monitoring the change of the optical path length in the arm of the interferometer passing through the fluid, while filling the SCU from vacuum to around the critical density. A homogeneous change in density is shown in an interferogram by a collective movement of the fringes in the field of observation in one direction. The interference order is proportional to the total geometrical path length in the fluid and the change in refractive index (see eq. (4.1)). Since, during filling, the refractive index changes from 1 to 1.09 approximately and the path length is about 20 mm, the interference order change is close to 3000! Thus, by counting fringes at an arbitrary location in an interferogram, the refractive index of the sample may in principle be found to within less than 0.5‰.

† This is of course limited by the requirement to keep the meniscus in the field of view.

In order to keep the fluid inside the SCU in single phase and to avoid density stratification in the sample (cfr. eq. (2.67)), the filling is performed at a temperature of 48 ˚C (approximately 2.5 ˚C above T_c). At this temperature, the sample content is homogeneous in both the start and end situation. Because the refractive index solely depends on the density and not on the temperature, eq. (4.1) may be used. Unfortunately, filling this way a meniscus cannot be utilized to establish whether the density is close enough to critical. Instead, the a near-critical density is attained on the basis of the corresponding pressure at 48 ˚C. A drawback of this procedure is that often, after lowering the temperature to below T_c, it was found that the position of the meniscus was outside the range for proper application for the accurate determination of z_m. In fact, the success score was very poor and a large series of trial fillings were required to obtain 17 runs.

An alternative procedure consists in determining the order change while emptying the SCU. The advantage of this is that the cell can be filled on the basis of the meniscus position. However it is of utmost importance that, when opening the valve to empty the cell and start the fringe counting, temperature and pressure are equal on both sides of the valve, so as not to induce a large disturbance in the fluid. Such a disturbance would result in chaotic fringe movement, making the change in interference order undetectable. It turns out to be extremely difficult to bring about this thermal equilibrium. Furthermore, in emptying, it was hard to assure a slow and smooth monotonous decrease in pressure. As it is, these experimental difficulties cause a large deterioration of accuracy in n (to about 3%). Therefore, the first procedure was preferred.

5.3 Meniscus position analysis

As discussed in chapter 3, the DER-SCU is a cylindrical cell the axis of which is, for the optical measurements, positioned horizontally. In this arrangement the meniscus will appear in the middle, when the sample is exactly at critical density. Therefore, in the analysis the data on the density and the refractive index obtained from the various runs were plotted as a function of the position of the meniscus. It is shown easily that for a cylindrical geometry, with the gravity vector perpendicular to the longitudinal axis, the average density (ρ_a) as a function of meniscus position is given by

$$\rho_a = \frac{1}{2}(\rho_l + \rho_v) + \frac{4}{\pi}(\rho_l - \rho_v)P - \frac{8}{3\pi}(\rho_l - \rho_v)P^3 + \dots , \tag{5.6}$$

where ρ_l and ρ_v are the densities for the liquid and the vapour phase respectively and $P \equiv z_m / D_c$, where D_c is the diameter of the cylinder. For small values of P eq. (5.6) is approximated by:

$$\rho_a - \rho_{CM} = \frac{4}{\pi}(\rho_l - \rho_v)P , \tag{5.7}$$

where $\rho_{CM} \equiv (\rho_l + \rho_v)/2$ is the average of the vapour and liquid densities. This average is described by the rule of Cailletet–Mathias:

$$\frac{\rho_l + \rho_v}{2\rho_c} = 1 + A|\tau| , \tag{5.8}$$

where $A = 0.722$ [36]. The linear expression of eq. (5.7) represents the relation between the deviation from ρ_{CM} and the meniscus position with a precision better than 1‰ for the range $-0.1 < P < 0.1$; for the range $-0.2 < P < 0.2$ the precision is still better than 1%.

When using eq. (5.7) in the interpretation of experimental data a practical problem arises, due to the fact that P has to be determined from an enlarged image of the cell on a screen. Since the THU and the optics are exchanged between measurement steps, the magnification cannot be fixed with sufficient precision. Therefore, in practise the meniscus position is scaled rather to the diameter of the circular calibration marker on the window (see section 3.3.3). Equation (5.7) then becomes

$$\rho_a - \rho_{CM} = \frac{4}{\pi}\frac{D_m}{D_c}(\rho_l - \rho_v)P_m, \tag{5.9}$$

where $P_m \equiv z_m / D_m$ and D_m is the diameter of the marker. Equation (5.9) shows that, plotting of ρ_a versus P_m for the various runs, ρ_{CM} can be obtained as $\rho_{CM} = \rho_a(P_m = 0)$. Subsequently, the critical density may be found by application of the rule of Cailletet–Mathias (eq. (5.8)) when A and τ are known.

Equation (5.9) also shows that the slope of such a plot is dependent on $(\rho_l - \rho_v)$, hence on the distance to the critical temperature (see eq. (2.12)). In fact, combining eqs. (2.12) and (5.9) we find for P_m-values at the same average density but at two different temperatures, τ_1 and τ_2:

$$P_m(\tau_1) = \left(\frac{\tau_2}{\tau_1}\right)^{\beta} P_m(\tau_2) - \frac{\pi}{4}\frac{D_c}{D_m}\frac{A}{2B}\frac{\tau_1 - \tau_2}{(-\tau_1)^{\beta}}. \tag{5.10}$$

Note that this relation is independent of ρ_a. Therefore, a plot of $P_m(\tau_1)$ versus $P_m(\tau_2)$ for the various runs is expected to be linear. This plot enables scaling of $P_m(\tau_1)$ and $P_m(\tau_2)$, to be discussed in section 5.4, in order to use all P_m-data (at both temperatures) in a single ρ_a versus P_m plot.

The critical density can be found also from the intersection of two plots ρ_a versus P_m for two different temperatures. According to eqs. (5.9) and (5.10) this intersection (P_i, ρ_i) is given by:

$$P_i = \frac{\pi}{4}\frac{D_c}{D_m}\frac{A}{2B}\frac{\tau_1 - \tau_2}{[(-\tau_2)^{\beta} - (-\tau_1)^{\beta}]}$$

$$\rho_i = \rho_c\left[1 - A\left\{\frac{|\tau_1|}{\left(\frac{\tau_1}{\tau_2}\right)^{\beta} - 1} + \frac{|\tau_2|}{\left(\frac{\tau_2}{\tau_1}\right)^{\beta} - 1}\right\}\right]. \tag{5.11}$$

The value for the critical density found in this way must agree, of course, with the values found by the previously mentioned method. A possible discrepancy might come from a wrongly assumed height for the position of the volumetric middle of the container. Such an incorrect height will not reveal itself directly out of the previously mentioned plots since it does not affect their slopes. Therefore, eq. (5.11) provides a means to check this height.

As shown in section 5.1, the relation between $n - n_c$ and $\rho - \rho_c$ is also expected to be linear. Hence n_c can be found analogous to the determination of ρ_c. Combining the (ρ_a, n, P_m)-data sets will finally also yield the required $n(\rho)$-relationship as will be discussed in section 5.4.

5.4 Results and discussion

Since the position of the meniscus at a certain average density depends on the temperature difference with T_c, we have to determine the distance to T_c at which we measure P_m. When using optical cells the general consensus is that T_c should be identified with the temperature at which the fluid is observed to decompose from one phase into a two-phase (liquid-vapour) system. Several difficulties, some experimental and some related to the properties of the fluid itself, may be encountered in the precise location of this phase separation. In general, the precision will always be limited by the thermal stability of the thermostat. With the excellent thermal stability of our THU however, it is the characteristic behaviour of the critical fluid, especially in the gravitational field, which limits the precision. In pure fluids in gravity, a major problem is the close phenomenological similarity of the continuous equilibrium density profile in the one-phase region to the discontinuous two-phase density profile. This similarity introduces some arbitrariness in the precise onset of phase separation, but the phenomenology could be reproduced to within 5 mK†. In view of this arbitrariness, it could well be that the actual value of T_c differs from the estimated value. We will come back to this later.

Table 5.2 Experimental results.

density	P_m at T_c -110 mK	P_m at T_c -30 mK	refractive index
736.511	-4.56		
747.202	11.27	14.55	
735.609	-5.36	-7.14	
742.898	3.46	5.38	
739.288	-1.65	-2.06	
739.705	0.41	2.24	
738.802	-1.57	-5.10	
740.399	1.69	2.97	
741.857	2.80	3.20	1.08724
	1.94	2.26	
	13.74	18.21	1.08819
	-60.30	-84.40	1.08174
	-37.20	-52.20	1.08386
734.151	-8.70	-12.90	1.08629
740.746	1.29	0.97	1.08711
732.068	-11.29	-16.45	1.08601
	-7.50	-10.40	

The experimental results are given in table 5.2. In fig. 5.1, the density measurements at T_c-110 mK from 12 runs are displayed versus the position of the meniscus, together with a linear fit through the data. This linear fit results in $\rho_{CM}(\tau_1)$=739.79±0.1 kg/m^3 and a slope of 68±2 kg/m^3, yielding ρ_c=739.61±0.1 kg/m^3. In fig. 5.2, the same 12 density measurements are displayed versus the meniscus position at T_c-30 mK. The linear fit now returns $\rho_{CM}(\tau_2)$=739.96±0.2 kg/m^3 with a slope of 47±3 kg/m^3, giving ρ_c=739.91±0.2 kg/m^3. This leaves us with an apparent difference in

† The scale of the measurement thermistor is absolute only to within 100 mK but is reproducible to within 100 μK. Since it was not the objective of this work to determine T_c, we did not bother to calibrate this thermistor.

the values of ρ_c between both temperatures, although just within the experimental error of both fits.

Figure 5.1 Density vs meniscus position.

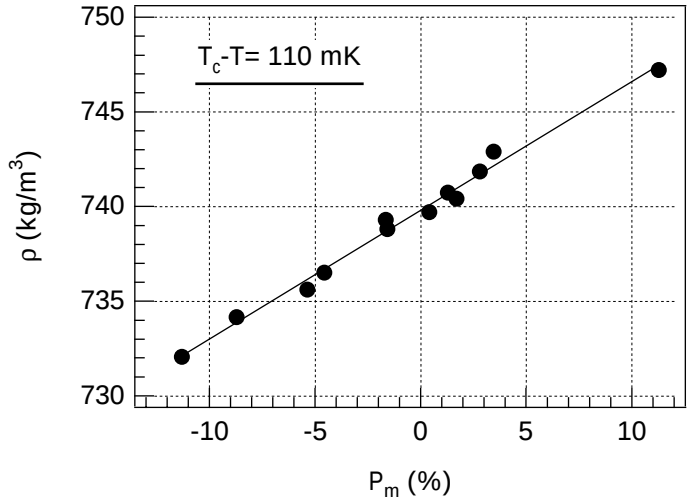

Figure 5.2 Density vs meniscus position.

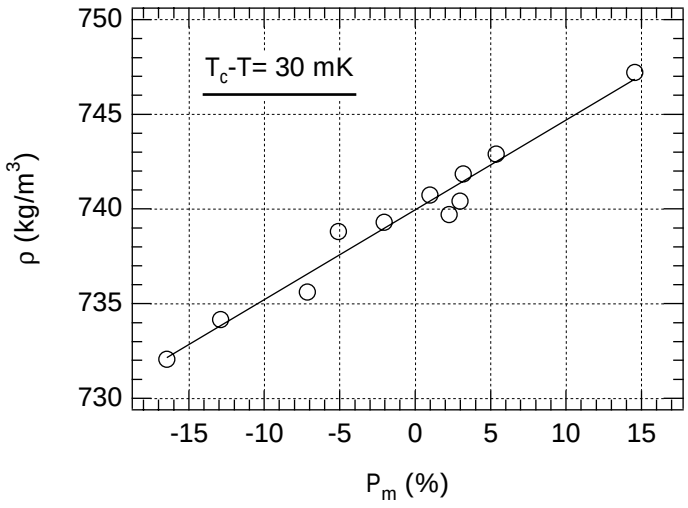

As a next step, we compare the values for the slopes (see eq. (5.9)) at these two temperatures to values that can be derived from the literature. To this end we calculate ρ_l and ρ_v from eq. (2.12), using values for the critical amplitude B and exponent β found experimentally for SF_6 by Jany and Straub [36]. With $B = 1.87$ and $\beta = 0.338$, the slope at T_c-110 mK is approximately 70 kg/m^3 and at T_c-30 mK is 45 kg/m^3. In view of the uncertainty in T_c, we consider this a fairly good agreement.

The reliability of the P_m data is assessed with the aid of eq. (5.10). We have plotted in fig. 5.3 $P_m(\tau_1 = 0.11/T_c)$-values vs. $P_m(\tau_2 = 0.03/T_c)$-values for 17 values of the average density. This plot demonstrates an excellent constant value for the slope of 0.717±0.01. However, on the basis of eq. (2.12) this figure is not consistent with the T_c-value estimated by observing the phase separation. To obtain consistency we have to assume a value β=0.256. Conversely, using the universal value β=0.325, we can estimate T_c on the basis of fig. 5.3 and eq. (2.12). In doing so, we find a

critical temperature which is only 15 mK higher than our estimated value; in view of the arbitrariness in the direct optical determination of the phase separation temperature (see the first paragraph of this section), such a systematic error is quite defendable. Hereafter we will use the latter value for T_c.

Figure 5.3 P_m at T_c-110 mK vs P_m at T_c-30 mK.

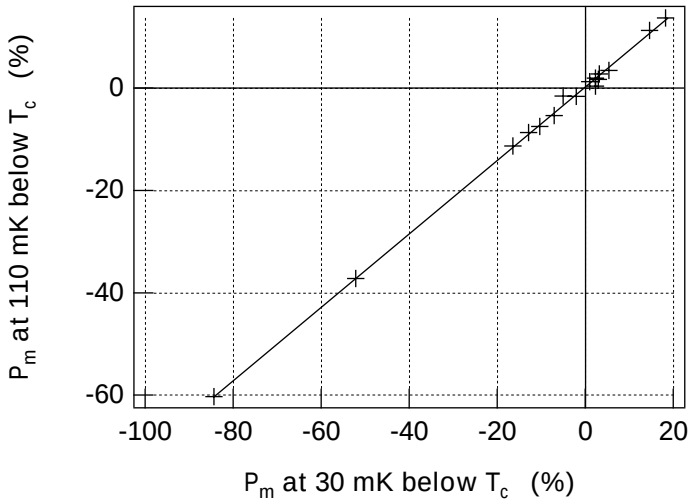

The newly identified T_c does not explain the apparent difference in values for ρ_c as found by the linear fits at both temperatures. This difference must be attributed to the finite accuracy by which the volumetric middle of the cell (cell axis) can be established. According to eq. (5.11) the fits in figs. 5.1 and 5.2 should intersect at P_m=-0.6%. However, P_i =0.8%, corresponding to a possible systematic error of 0.095 mm in the determination of the cell axis. As this discrepancy lies within the experimental error, we have chosen to shift our calibration accordingly in order to obtain self-consistency of our data. If we subtract 1.4% from the P_m-values, a fit of $P_m(\tau_1)$ versus $P_m(\tau_2)$ yields:

$$P_m(\tau_1) = (0.717 \pm 0.008) P_m(\tau_2) - (1.4 \pm 2) \cdot 10^{-3}, \tag{5.12}$$

nicely corresponding to the offset given in eq. (5.10). If we scale the P_m-values at τ_2 to a value at τ_1 on the basis of eq. (5.12) and fit to a unified (ρ_a, P_m)-plot (see fig. 5.4), the result is:

$$\rho_a = 740.73 \pm 0.14 + (67 \pm 2) P_m . \tag{5.13}$$

The corresponding critical density to this fit is $\rho_c = 740.52 \pm 0.14$ kg/m^3. To the uncertainty in the critical density we have to add the uncertainty in the calculated volume of the container, i.e. 0.025%. Therefore, we find

$$\rho_c = 740.5 \pm 0.3 \text{ kg/m}^3 . \tag{5.14}$$

Analogously, by plotting the data of 7 runs n versus P_m we find for the critical refractive index

$$n_c = 1.087122 \pm 1.3 \cdot 10^{-5} . \tag{5.15}$$

Figure 5.4 A unified plot of ρ_c versus P_m.

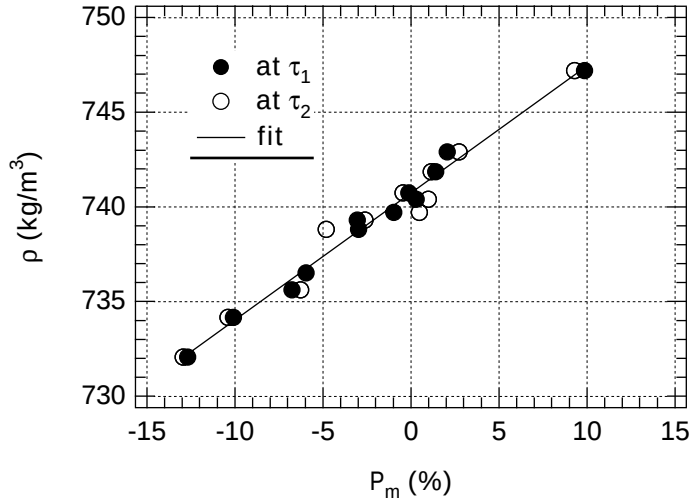

Finally we plot values for the refractive index from seven runs versus the corresponding ρ_a-values, of which three are obtained from P_m-values inserted in eq. (5.13). This plot, together with the linear fit, is shown in fig. 5.5. The result is:

$$n = n_c + K(\rho - \rho_c)$$
$$K = (1.29 \pm 0.01) \cdot 10^{-4}\ \mathrm{m^3/kg}\ . \qquad (5.16)$$

Figure 5.5 Refractive index (n) vs density (ρ).

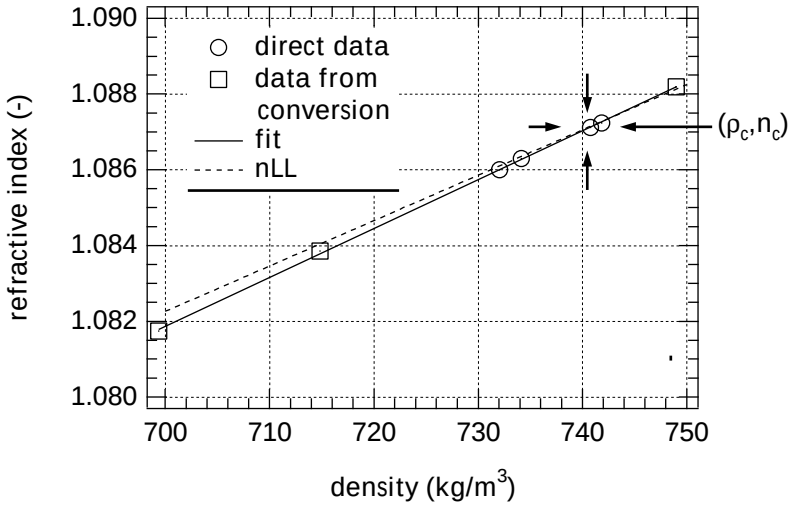

It can be seen from table 5.1 that our experimental value for ρ_c fits well within the range of literature data. The value for n_c from our experiment seems rather low. The latter may possibly be attributed to the fact that, as discussed in section 5.1, in the interpretation of refractive index data quite commonly the Lorentz–Lorenz relation is involved. This relation can be used to predict with some accuracy the value of n_c if ρ_c is known (e.g., judging from table 5.1, with an accuracy of 0.5%). However, one cannot infer similar accuracies for n_c-1, nor so for the derivative $(dn/d\rho)_{\rho = \rho_c}$. For such quantities the accuracy is reduced by typically an order of magnitude.

To stress this point, we have plotted in fig. 5.5 n_{LL}, which is the 'theoretical' refractive index curve, based on our experimental n_c, ρ_c and the corresponding value for the Lorentz–Lorenz constant as given by eq. (5.1), which amounts to $Q = 7.717 \cdot 10^{-5}$. The corresponding slope then is $1.20 \cdot 10^{-4}$ m^3/kg, which differs about 7% from our experimental value.

To conclude, the experiment described in this chapter has provided, in a straightforward way, accurate and independent data on the critical density and the critical refractive index, together with the $n(\rho)$ dependence for the critical region. Our results show that, in contrast to the experimental practise, in the critical region of SF_6 one should be careful in using the Lorentz–Lorenz relation when the value for the derivative $(dn/d\rho)$ is important for the interpretation of experimental results.